An improved model of hardening gear wheels and determining the electrical efficiency of the process

1st Jerzy Barglik
Faculty of Material Engineering
Silesian University of Technology
Katowice, Poland
jerzy.barglik@polsl.pl

2nd Václav Kotlan
Faculty of Electrical Engineering
University of West Bohemia
Pilsen, Czech Republic
vkotlan@fel.zcu.cz

3rd Albert Smalcerz
Faculty of Material Engineering
Silesian University of Technology
Katowice, Poland
albert.smalcerz@polsl.pl

4th Adrian Smagór
Faculty of Material Engineering
Silesian University of Technology
Katowice, Poland
adrian.smagor@polsl.pl

5th Debela Desisa
Faculty of Material Engineering
Silesian University of Technology
Katowice, Poland
Debela.Desisa@polsl.pl

6th Ivo Doležel
Faculty of Electrical Engineering
University of West Bohemia
Pilsen, Czech Republic
idolezel@fel.zcu.cz

***Abstract*—The paper presents an improved model of induction hardening of gear wheels. Although the mathematical model of the hardening is well known, some parameters are subject to uncertainties (temperature dependence of material parameters, coefficient of convective heat transfer, or emissivity). The authors offer a methodology based on calibration and optimization techniques to minimize the relevant errors and illustrate it with a typical example.**

***Index Terms*—gear wheels, hardening, calibration, optimization, mathematical model**

I. Introduction

From the mathematical viewpoint, induction hardening is typically a coupled task that involves a non-linear interaction between magnetic and temperature fields. It also results in metallurgical changes, especially in the surface structures of the material being processed [1]. Induction hardening is commonly performed in a three-dimensional configuration, making optimizing its input parameters practically challenging.

Due to this difficulty, it becomes necessary to introduce appropriate simplifications, which can significantly expedite the computations. However, a question regarding the reliability and accuracy of such a simplified model arises. To address this concern, the model must undergo thorough calibration to ensure that the results fall within the tolerance range of the experimental data.

II. Solution Procedure

The simplified model starts from the following assumptions: It considers that the temperature Ac_3 does not depend on the heating rate, and the continuous cooling transform (CCT) diagram remains unaffected by it, too. The variations in the material microstructure are considered only qualitatively. The procedure of teeth cooling, whether by spraying or natural air circulation, works with a constant or linearly dependent convection coefficient. It must, however, correspond to the real cooling time [2]. The way of finding this coefficient is the main contribution of this paper, as its value is necessary to model the quenching process of similar wheels.

We assume that the dimensions of the wheel and inductor are known so that we may only optimize the amplitude and frequency of the field current, together with the convective coefficients. The converter's frequency, however, can only vary within a narrow range (although we can perform the sweep analysis within a narrower band to find its optimal value), so it is often sufficient to optimize only the time evolution of the current envelope. The convection coefficients can be determined experimentally from the temperature measured at several points on the tooth (its tip, root, and center) for two different values of the field current. Then, we process the results using powerful optimization techniques [3] to find the required temperature pattern of the hardened layers.

III. Mathematical Model

The induction hardening process of a gear wheel comprises two sub-processes. The first sub-process involves induction heating, achieved using a one-turn circular pipe-type copper inductor cooled by water. Once the surface layers of the wheel reach the desired temperature for hardening, which exceeds Ac_3 for the material used, the cooling process begins. An appropriate quenchant, such as water or polymer, cools the wheel, or it can cool naturally in the air. The hardness of the resulting surface layers follows from the cooling time, where faster cooling leads to higher hardness.

The fundamental equation governing the process of heating may be written as [4]:

$$\operatorname{curl}\left(\frac{1}{\mu}\cdot\operatorname{curl}\boldsymbol{A}\right)+\gamma\cdot\frac{\partial\boldsymbol{A}}{\partial t}=\boldsymbol{J}_{\mathrm{ext}}. \tag{1}$$

This research was funded by the Silesian University of Technology, grants No. 11/040/BK_21/0023 and 11/040/BKM21/0025 and supported by the National Center for Research and Development, grant number PBS2/A5/41/2014. On the Czech side, the research was supported by the Technological Agency of the Czech Republic, project No. FW06010523.

Here, symbol $\boldsymbol{A}$ denotes the magnetic vector potential, γ stands for the electric conductivity, μ is the magnetic permeability, and $\boldsymbol{J}_{\mathrm{ext}}$ represents the external current density in the inductor that is considered uniform. The boundary conditions applied along an artificial boundary are of Dirichlet's or Neumann's kind.

The temperature field is described by the heat transfer equation in the form [4]:

$$\operatorname{div}\,(\lambda \cdot \operatorname{grad}\ T) = \rho \cdot c_{\mathrm{p}} \cdot \frac{\partial T}{\partial t} - p_{\mathrm{J}}. \tag{2}$$

Here, symbol λ denotes the thermal conductivity, ρ represents the specific mass, T is the temperature, c_{p} stands for the volumetric heat, and p_{J} denotes the volumetric Joule losses. The boundary conditions include convection and radiation, but for the sake of simplicity, the influence of radiation is incorporated into the impact of convection.

Equation (2) still characterizes the cooling process, but the second term on the right side disappears as there are no energy losses within the body. The boundary condition is similar to the heating case, albeit with distinct coefficients.

A hard-coupled formulation must be used to solve equations (1) and (2) because the material properties are highly nonlinear and vary with temperature. Additionally, the magnetic permeability of hardened steel relies not only on temperature but also on the magnetic flux density and frequency applied.

Since the specific details of the model have been extensively covered in various references ([5] or [6]) and are generally well-known, they will not be further analyzed here. Instead, the focus will be on the coefficient α representing convective heat transfer, which is typically estimated and becomes particularly challenging to determine precisely when employing more aggressive cooling techniques (such as spraying or immersing the heated body in a cold quenchant). Therefore, it is crucial to calibrate the model appropriately for reliable results.

Careful temperature measurements must be conducted at specific points on the teeth to calibrate the model. The cooling rate derived from these measurements is then utilized to determine the temperature dependency of the coefficient α.

Another challenge arises when seeking the final hardness profile of the tooth. Typically, this value may be obtained from the Continuous Cooling Transformation (CCT) diagram of the steel used. However, constructing the CCT diagram involves a prescribed heating method and adjusted values of temperatures like Ac_3 and Ac_1. It is important to note that these temperatures depend not only on the heating rate but also on the chemical composition of the steel, which can vary from manufacturer to manufacturer. As a result, slightly different CCT diagrams can be found for the same type of steel. Specialized equipment is required to measure the dependence of Ac_3 and Ac_1 on the heating rate for each steel component provided by the manufacturer. These data enable obtaining a heating rate that corresponds to the actual process.

IV. Illustrative Example

The methodology is exemplified by demonstrating the induction-hardening process of a gear wheel made of AISI 4340 steel. Figure 1 illustrates the wheel's fundamental dimensions with other pertinent information in Table 1.

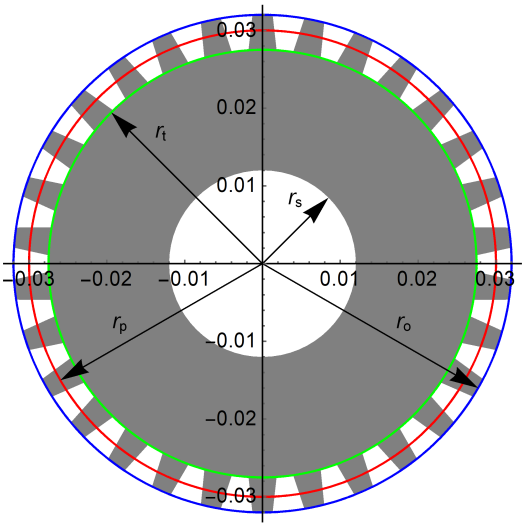

Fig. 1. Principal geometry of the gear wheel

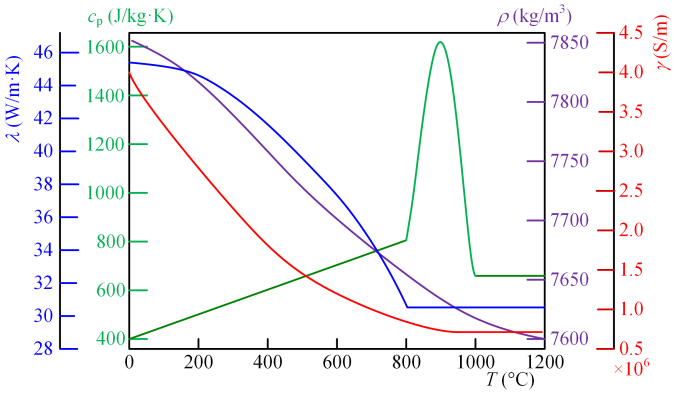

Fig. 2. Temperature dependencies of the parameters of steel AISI 4340

Table 1. Main dimensions of the gear wheel

Quantity	Symbol	Value	Unit
Number of teeth	N	30	-
Shaft radius	r_{s}	12	mm
Root radius	r_{t}	27.5	mm
Pitch circle radius	r_{p}	30	mm
Outer radius	r_{o}	32	mm
Wheel thickness	h	7.5	mm

Figure 2 shows the temperature-dependent physical parameters of steel AISI 4340 (thermal conductivity λ, electric conductivity γ, volumetric heat c_{p}, and specific mass ρ) [7]. These are used as input data for the computations.

A. Heating

The experimental work was realized at the specialized laboratory stand located at the Silesian University of Technology [8]. First, we modeled the process of induction heating. The source current had an amplitude $I_{\mathrm{m}} = 1.136\,\mathrm{kA}$, and its

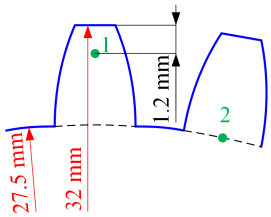

Fig. 3. Positions of thermocouples 1 and 2 (they are built in two neighbor teeth to avoid influencing one another)

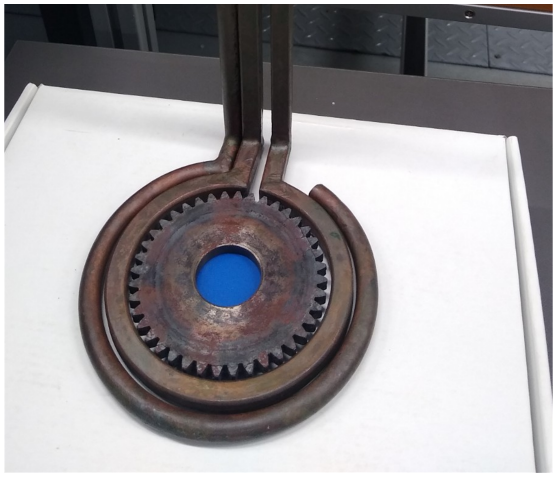

Fig. 4. Arrangement of wheel hardening (the gap between wheel and inductor is 1 mm, external cylindrical circular pipe is the sprayer)

frequency was $f = 32.07\,\mathrm{kHz}$. The heating time to the required temperature above $850\,^{\circ}\mathrm{C}$ (providing practically $100\,\%$ austenite solution in the surface layers of the teeth) was $7.0\,\mathrm{s}$. The time evolution of the temperature was measured by two thermocouples placed at a depth of 1.2 mm below the top of the tooth and in its root (see Fig. 3).

The arrangement of heating is shown in Fig. 4. The inductor is supplied from an inverter through the busbars and massive hollow conductors.

The efficiency η of the process of heating the wheel can be determined from the model using the formula

$$\eta = \frac{Q}{W_\mathrm{e}} = \frac{\int_0^V \left[\int_{T_0}^T \rho \cdot c_\mathrm{p} \cdot \mathrm{d}T\right] \mathrm{d}V}{\int_0^{t_\mathrm{k}} u \cdot i \cdot \mathrm{d}t}. \tag{3}$$

Here, Q is the heat delivered to the wheel, W_e stands for the electric energy consumed by the system inductor-wheel (and possibly the sprayer), V represents the wheel volume and T denotes the distribution of the final temperature at the end of heating. Furthermore, the symbol T_0 is the initial temperature of the wheel before heating, $\rho(T)$ is its specific gravity, $c_\mathrm{p}(T)$ is its volumetric heat at constant pressure, $u(t)$ is the secondary voltage of the transformer, $i(t)$ is the current of the secondary winding supplying the inductor and t_k is the heating time.

The supplying circuit may be described by the equation

$$u = R \cdot i + \frac{\mathrm{d}\,(L \cdot i)}{\mathrm{d}t}. \tag{4}$$

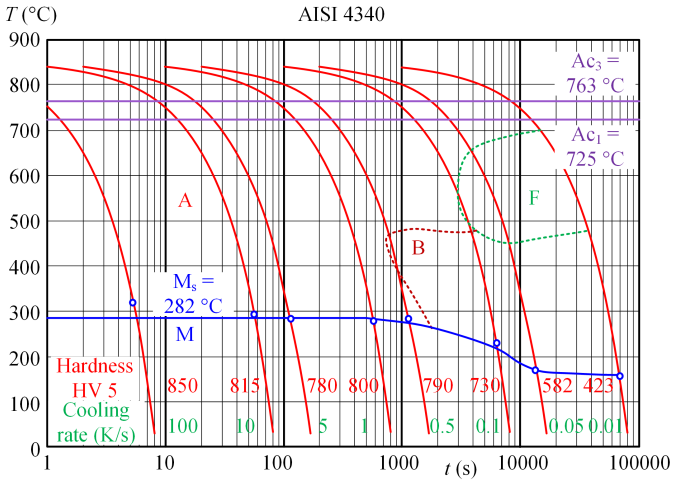

Fig. 5. CCT diagram of steel AISI 4340: A–austenite, M–martensite, F–ferrite, B–bainite [9]

This way of calculating the integral in the denominator of (3) seems to be the best for calculating the electric energy delivered to the system, as the direct measurement of the active power would be problematic because of a low value of the power factor φ. Then

$$\int_0^{t_\mathrm{k}} u \cdot i \cdot \mathrm{d}t = \int_0^{t_\mathrm{k}} R \cdot i^2 \cdot \mathrm{d}t + \int i \cdot \mathrm{d}\,(L \cdot i)\,. \tag{5}$$

The resistance and inductance of the system busbar-feeder-inductor-sprayer were measured very carefully during the whole process of heating, using a precise RLC meter. Their mean values in time were $R = 5.84\,\mathrm{m\Omega}$ and $L = 274\,\mathrm{nH}$. The inductance is, however, negligibly small compared with the resistance, and its influence can be neglected.

Then

$$W_\mathrm{e} = \frac{R \cdot I_\mathrm{m}^2 \cdot t_\mathrm{k}}{2} = 31.94\,\mathrm{kWh}, \tag{6}$$

while the value of Q in (3) obtained from the numerical calculation of the temperature distribution in the gear wheel at the end of heating is $7.92\,\mathrm{kWh}$. The computations were carried out by the finite element method, and the integral in the numerator of (3) was obtained by summing up the individual contributions in all the time subintervals and all elements. Hence, $\eta = Q/W_\mathrm{e} = 0.248$.

B. Cooling

The cooling starts from the CCT diagram of steel AISI 4340 depicted in Fig. 5.

The next step is the calibration of coefficient α. It consists of four following sub-steps:

1) Proposal of the objective function f in the form $f = \sum_{i=1}^{n} (T_{ci} - T_{\mathrm{m}i})^2$, where n is the number of the selected points, $T_{\mathrm{m}i}$ are the measured, and T_{ci} the calculated values of temperature at these points.
2) Selection of suitable optimization methods. After thorough testing, we chose the BOBYQA procedure.

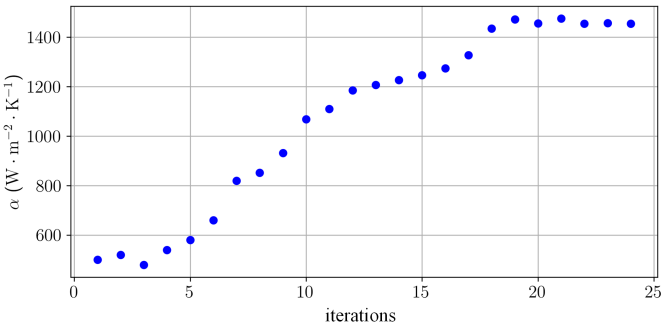

Fig. 6. Convergence of coefficient α (its initial value being 500)

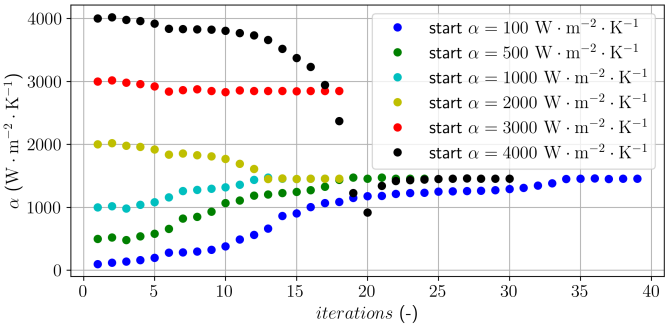

Fig. 7. Convergence of coefficient α for different initial values

3) Repeated applications of this procedure for different initial values of α and comparison of results.

The resulting coefficient α for fast cooling is $1485\,\mathrm{W{\cdot}m^{-2}{\cdot}K^{-1}}$. Its value was calculated after only twenty iterations with the BOBYQA algorithm. Figure 6 shows the convergence of α in the dependence on iterations. The initial value was $\alpha = 500\,\mathrm{W{\cdot}m^{-2}{\cdot}K^{-1}}$.

Similar convergence patterns we obtained for different initial values of α; see Fig. 7. The only exception occurs when the initial value of α is $2300 - 3000\,\mathrm{W{\cdot}m^{-2}{\cdot}K^{-1}}$. The objective function has another extreme for this value visible even from the convergence curve for $\alpha = 4000\,\mathrm{W{\cdot}m^{-2}{\cdot}K^{-1}}$; a steep change is notable at this place. The most probable reason is that the objective function is wavy and has more extremes there.

Finally, Fig. 8 shows the comparison of the measured and calculated cooling curves at the thermocouples TC1 and TC2 for $\alpha = 1485\,\mathrm{W{\cdot}m^{-2}{\cdot}K^{-1}}$. It is evident that the agreement is very good, and particular differences do not exceed more than about 6 %.

V. Conclusion

The paper describes an enhanced approach to induction hardening that starts by determining a more accurate heat transfer coefficient. This coefficient is often unknown when aggressive cooling methods such as spraying or sinking into a quenchant are employed.

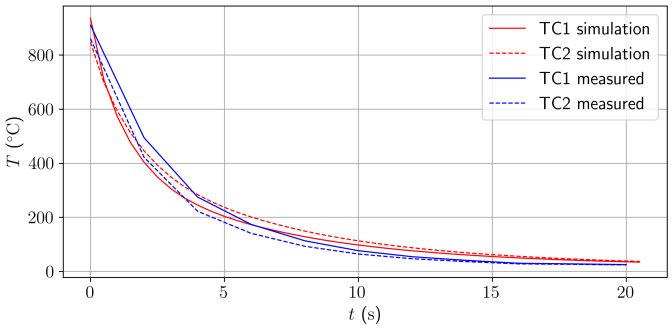

Fig. 8. Comparison of measured and calculated cooling curves

The authors propose a method starting by measuring the temperature evolution at specific spots of the heated body using thermocouples. The data obtained are subject to an optimization process to determine the coefficient values that ensure the most similar temperature evolution and cooling time. The authors utilized the BOBYQA method for optimizing and demonstrated its advantages for modeling gear wheel hardening. Additionally, they calculated an electric efficiency of about 0.25 for the heating process.

Nevertheless, using deterministic algorithms for optimizing the convective coefficient requires considerable attention. The objective function often exhibits more local extremes, and the result may be faulty. So it is necessary to compare it automatically with measured data. Only a precise experiment may confirm its correct value.

Future research in this field will concentrate on expediting the algorithms used, as the optimization process alone takes over 30 hours when executed on a cluster comprising four high-performance computers.

References

[1] J. Grum, Induction hardening. In: Handbook of residual stress and deformation of steel, G.F. Totten, M.A.H. Howes, and T. Inoue, Eds. ASM International, Materials Park, pp. 220–247, 2002.

[2] V. Kotlan, I. Petrasova, and I. Dolezel, "Usage of continuous cooling transformation (CCT) diagrams for laser and small-scale induction hardening," J. Comput. Appl. Math., vol. 428, paper 115123, 2023.

[3] P. Karban, D. Panek, T. Orosz, I. Petrasova, and I. Dolezel, "FEM based robust design optimization with Agros and Ārtap," Comput. Math. Appl., vol. 81, pp. 618–633, 2021.

[4] J. Barglik, A. Smagor, and A. Smalcerz, "Induction hardening of gear wheels of steel 41Cr4," Przeglad Elektrotechniczny, vol. 57, pp. S3–S12, 2018.

[5] M. Areitioaurtena, U. Segurajauregi, M. Fisk, M. J. Cabello, and E. Ukar, "Numerical and experimental investigation of residual stresses during the induction hardening of 42CrMo4 steel.," Eur. J. Mech. A/Solids, vol. 96n paper 104766, 2022.

[6] J. Chovan, Ch. Geuzaine, and M. Slodicka, "*A-Φ* formulation of a mathematical model for the induction hardening process with a nonlinear law for the magnetic field," Comput. Methods Appl. Mech. Eng., vol. 2, pp. 294–315, 2017.

[7] E.H. Boyer and T.L. Gall, Eds., Metal Handbook. American Society for Metals, Material Park, OH, 1985.

[8] J. Barglik, A. Smalcerz, A. Smagor, and G. Kopec, "Experimental stand for investigation of induction hardening of steel elements," Metalurgija, vol. 57, pp. 341–344, 2018.

[9] M. Eckert, M. Krbata, M. Barenyi, J. Majerik, A. Dubec, and M. Bokes, "Effect of selected cooling and deformation parameters on the structure and properties of AISI 4340 steel," Mater., vol. 13, paper 5585, 2020.